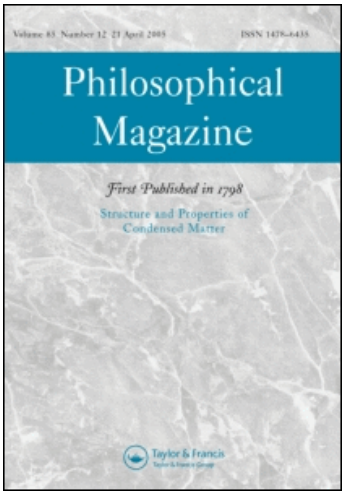

Philosophical Magazine
Publication details, including instructions for authors and subscription information:
http://www.informaworld.com/smpp/title~content=t713695589

The crucial role of chemistry on mobile properties of dislocation

Zhengzheng Chen[a]; Gang Lu[a]; Nicholas Kioussis[a]; Nasr M. Ghoniem[b]
[a] Department of Physics, California State University, Northridge, CA 91330-8268 [b] Department of Mechanical and Aerospace Engineering, University of California Los Angeles, CA 90095

First published on: 12 May 2010

To cite this Article Chen, Zhengzheng , Lu, Gang , Kioussis, Nicholas and Ghoniem, Nasr M.(2010) 'The crucial role of chemistry on mobile properties of dislocation', Philosophical Magazine, 90: 27, 3757 — 3765, First published on: 12 May 2010 (iFirst)
To link to this Article: DOI: 10.1080/14786430903369577
URL: http://dx.doi.org/10.1080/14786430903369577

Philosophical Magazine
Vol. 90, Nos. 27–28, 21–28 September 2010, 3757–3765

Taylor & Francis
Taylor & Francis Group

The crucial role of chemistry on mobile properties of dislocation

Zhengzheng Chen[a]*, Gang Lu[a], Nicholas Kioussis[a] and Nasr M. Ghoniem[b]

[a]*Department of Physics, California State University, Northridge, CA 91330-8268;*
[b]*Department of Mechanical and Aerospace Engineering, University of California Los Angeles, CA 90095*

(*Received 7 April 2009; final version received 21 September 2009*)

Dislocation–solute interactions are ubiquitous in solids, yet their dual nature in strengthening or softening the material is not well understood. Results of a novel concurrent multiscale approach reveal that the *local environment* of W solutes in Ta has a dramatic effect both on the dislocation mobility and slip paths. W solutes can enhance or reduce the mobility, and may result in spontaneous dislocation glide. The atomistic mechanism responsible for the dual nature of solutes is elucidated.

Keywords: multiscale simulation; dislocations; impurity; chemistry effect

1. Introduction

Solute atoms are ubiquitous in metals and play a key role in altering their mechanical properties (e.g. strength, ductility). Experimental studies during the past several decades indicate that solutes can give rise to both solid-solution hardening (SSH) and softening (SSS) [1,2]. Since plastic deformation in metals is mediated by the motion of line defects (dislocations) that produce a long-range stress, the dislocation–solute interaction is of great practical importance. In most situations, dislocation behavior is considerably different in the realistically *dirty* materials, where dislocation mobility can vary by several orders of magnitude, depending on the type, concentration, and local environment of the solute.

Continuum elasticity theory has provided considerable insight in describing the long-range effects associated with mismatch in size and elastic constants between the solute and host atoms. On the other hand, the nonlinear short-range interactions between the solute and the dislocation core, which are of *chemical* or electronic origin [3,4], can have a dramatic effect on the dislocation core and hence the mobility. However, the understanding of the physics of dislocation–solute interactions remains a challenging problem due to the lack of predictive atomistic methods.

The bcc refractory metals (Nb, W, Ta, and Mo) exhibit unique mechanical properties that make them attractive for structural applications at elevated temperatures. An inherent drawback limiting the use of these materials as structural components is their reduced low-temperature toughness, which in turn increases the propensity towards fracture. Thus, the challenge in design of advanced alloys is to

*Corresponding author. Email: chenz@csun.edu

ISSN 1478–6435 print/ISSN 1478–6443 online

DOI: 10.1080/14786430903369577
http://www.informaworld.com

combine strengthening and toughening phases with a better balance of properties. Experimental studies have shown [1] that solid solutes have a dual nature, namely, they can soften (harden) the alloy at low (high) concentrations at a given temperature. For example, the addition of 2.5–10.0 wt.% W solutes to Ta increases the strength while it enhances substantially the ductility at high strain-rates, making the alloy more like Cu, a typical fcc metal [5,6].

In the present work, we employ a novel concurrent multiscale approach to study the effects of chemistry and local environment on the mobility of dislocations including the Peierls stress and Peierls potential in Ta-W alloys. This approach correctly treats the long-range elastic field of the dislocation and describes the solute–host atomic interaction in the core region accurately. The results demonstrate the dual nature of W solutes: depending on the solute local environment (random solid solution or nanoclusters of different geometry and composition), the mobility and/or Peierls potential may exhibit a wide spectrum of unusual behavior: SSH, SSS or even the disappearance of the Peierls potential resulting in a spontaneous dislocation glide in the absence of external stress. Finally, W solutes can serve as obstacles to dislocation motion and activate new slip planes.

2. Model and methodology

2.1. *Details of methodology*

The concurrent multiscale approach is based on that proposed by Choly et al. [7]. The system, shown in Figure 1, is divided into: Region I, which includes the dislocation core and the solutes, is treated within the framework of density functional theory (DFT); region II, which refers to the rest of the system, is treated with the embedded atom method (EAM) or Finnis–Sinclair (FS) potentials; and the boundary (**B**) region, introduced to reduce the coupling errors between regions I and II, respectively. The total energy of the system can be written [7],

$$E[\mathrm{I}+\mathrm{II}] = E_{\mathrm{DFT}}[\mathrm{I}] + E_{\mathrm{EAM}}[\mathrm{II}] + E^{\mathrm{int}}[\mathrm{I},\mathrm{II}]. \tag{1}$$

Here, $E_{\mathrm{DFT}}[\mathrm{I}]$ is the energy of region I in the absence of region II obtained by DFT calculations, $E_{\mathrm{EAM}}[\mathrm{II}]$ is the energy of region II obtained by EAM calculations in the absence of region I, and $E^{\mathrm{int}}[\mathrm{I}, \mathrm{II}]$ represents the interaction energy added to give the correct total energy of the whole system. In the present approach $E^{\mathrm{int}}[\mathrm{I}, \mathrm{II}]$ is calculated by the EAM potential,

$$E^{\mathrm{int}}[\mathrm{I},\mathrm{II}] = E_{\mathrm{EAM}}[\mathrm{I}+\mathrm{II}] - E_{\mathrm{EAM}}[\mathrm{I}] - E_{\mathrm{EAM}}[\mathrm{II}]. \tag{2}$$

This treatment of the interaction energy yields the following expression for the total energy,

$$E[\mathrm{I}+\mathrm{II}] = E_{\mathrm{EAM}}[\mathrm{I}+\mathrm{II}] - E_{\mathrm{EAM}}[\mathrm{I}] + E_{\mathrm{DFT}}[\mathrm{I}], \tag{3}$$

where $E_{\mathrm{EAM}}[\mathrm{I}+\mathrm{II}]$ is the energy of the entire region calculated from the EAM, and $E_{\mathrm{EAM}}[\mathrm{I}]$ and $E_{\mathrm{DFT}}[\mathrm{I}]$ are the energies of region I in the absence of II obtained by EAM and DFT calculations, respectively.

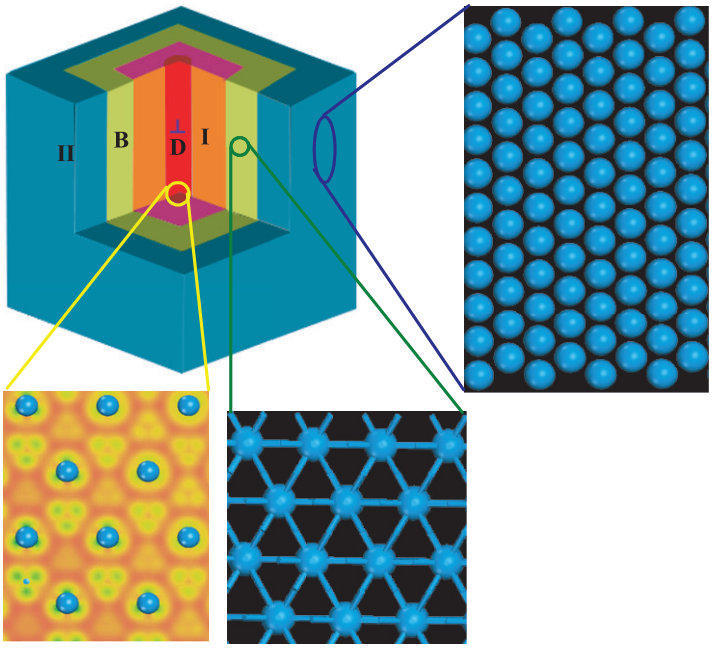

Figure 1. Schematic view of the partitioned multiscale system: region I (red online) contains the core of the screw dislocation (dark red marked by D); region II (blue online) consists of atoms treated with EAM; and the boundary (B) region (green online) consists of atoms on the boundary between regions I and II. Periodic boundary conditions are used along the ⟨111⟩ dislocation line.

Differentiation of Equation (3) with respect to the atomic positions $\mathbf{R}^{\mathrm{I}}$ and $\mathbf{R}^{\mathrm{II}}$ in regions I and II, respectively, yields that the forces on the DFT and EAM atoms are,

$$\begin{cases} F_i[\mathrm{I}] = -\dfrac{\partial E[\mathrm{I}+\mathrm{II}]}{\partial R_i^{\mathrm{I}}} = F_i^{\mathrm{EAM}}[\mathrm{I}+\mathrm{II}] - F_i^{\mathrm{EAM}}[\mathrm{I}] + F_i^{\mathrm{DFT}}[\mathrm{I}] \\ F_i[\mathrm{II}] = -\dfrac{\partial E[\mathrm{I}+\mathrm{II}]}{\partial R_i^{\mathrm{II}}} = F_i^{\mathrm{EAM}}[\mathrm{I}+\mathrm{II}]. \end{cases} \tag{4}$$

Equation (4) shows that the forces on the atoms in region II are solely determined by the EAM potential while those on the atoms in region I have several contributions. The boundary between regions I and II introduces a fictitious surface which in turn gives rise to substantial ghost forces on the atoms which lie in the vicinity of the boundary, namely in region **B**. These forces, which are due to the mismatch in the DFT and EAM forces on the surface atoms and the fictitious surface, severely degrade the accuracy of the approach. In order to improve the quality of the coupling across the boundary we have proposed an improved coupling scheme in our previous work [8]. The correction force on the atoms in **B** is

$$F_i^{\mathrm{corr}}[\mathbf{B}] = -F_i^{\mathrm{DFT}}[\mathbf{B}] + F_i^{\mathrm{EAM}}[\mathbf{B}], \tag{5}$$

yielding

$$F_i[\mathbf{B}] = F_i^{\mathrm{EAM}}[\mathrm{I} + \mathrm{II}] \tag{6}$$

for the force on these atoms. The introduction of the correction force requires the corresponding correction of the total energy E_{tot} of the entire system to guarantee the consistency between the forces and the energy. Thus, the total energy E_{tot} becomes

$$E_{\mathrm{tot}} = E[\mathrm{I} + \mathrm{II}] - \sum_{i \in \mathbf{B}} F_i^{\mathrm{corr}}[\mathbf{B}] \cdot u_i[\mathbf{B}], \tag{7}$$

where, $u_i[\mathbf{B}]$ is the displacement of a boundary atom at each relaxation step and the sum is over all atoms in **B**. E_{tot} is minimized by employing conjugate gradient techniques until the maximum force is smaller than 0.01 eV/Å.

2.2. *Atomic model*

The size of the entire system is 251 Å × 145 Å × 2.86 Å along the ⟨110⟩, ⟨112⟩, and ⟨111⟩ directions, respectively, containing 5400 atoms. Region I is 22 Å × 28 Å × 2.86 Å and contains 96 atoms. All atoms are initially displaced according to the isotropic elastic solution of the screw dislocation with Burgers vector $\vec{b} = \langle 111 \rangle a/2$, then are relaxed by the concurrent multiscale approach which takes into account the anisotropic effects. Periodic boundary conditions are applied along the ⟨111⟩ direction and fixed boundary conditions are employed along the other two directions, respectively. The DFT cluster calculations in region I were carried out using the VASP code [9,10]. We have used a 1×1×8 *k*-mesh according to the Monkhorst–Pack scheme [11]. The generalized gradient approximation functional [12] is used to treat the exchange and correlation potential, and the cutoff energies are set at 240 eV for both Ta and W. The EAM calculations employed the Ackland potential [13] for pure Ta and the Johnson scheme [14] for constructing the Ta-W interatomic potential. It should be emphasized that the quality of the Ta-W classical interaction is not crucial in this multiscale approach, due to the cancellation between the first two energy terms in Equation (3), provided that the various atomic species are well within region I. The external strain is applied by displacing equally the atoms in the outermost $(10\bar{1})$ and $(\bar{1}01)$ planes along the $[\bar{1}\bar{1}\bar{1}]$ and [111] directions, respectively. The corresponding shear stress, σ_{yz}, is calculated as the component of the area-averaged force on the surfaces parallel to the Burgers vector.

The presence of free surfaces in fixed boundary condition introduces image forces (F_{img}) [15], which depend on the dislocation position within the simulation box. F_{img} with continuum elasticity theory is given by [16]

$$F_{\mathrm{img}} = -\frac{\mu b^2}{4\pi}\left(\frac{1}{d_1} - \frac{1}{d_2}\right), \tag{8}$$

where μ is the shear modulus of Ta, b is the magnitude of the Burgers vector and d_1 and d_2 are the distances of the dislocation from the two surfaces, respectively. As pointed out by Domain [15], the image forces due to the two surfaces almost cancel out when the dislocation is around the center of the whole system. In the present work, the screw dislocation moves around the center. The maximum distance from

the center d_{max} is $3b$. Thus F_{img} has marginal effect on the simulation result of Peierls stress.

3. Results and discussion

In Figure 2 we show the relaxed dislocation core structure in pure Ta under zero stress (left panel) and 1.8 GPa (right panel), respectively, using the differential displacement (DD) maps [17]. The arrows indicate the relative ⟨111⟩ displacement of neighboring atoms of the dislocation. The length (direction) of the arrow denotes the magnitude (sign) of the displacement difference. When the arrow touches the centers of the two atoms, their relative displacement is $b/3$. The dislocation core for pure Ta is non-degenerate and spreads symmetrically on the six planes. Upon increasing σ_{yz} on the $(10\bar{1})$ planes, the dislocation center moves to the next Peierls valley at the critical stress σ_P of 1.8 GPa. Comparison of σ_P and the core structure in Table 1 employing different approaches, demonstrates that the concurrent multiscale approach is in excellent agreement with the results of the FP-GFBC method [18].

In order to study the effect of local environment of the solute on the mobility of the screw dislocation we have considered the cases of: (i) dilute random solid solutions where the dislocation line is affected only by isolated solute atoms (ISA) shown in Figure 3a, and (ii) small clusters of solute atoms of hexagonal shape (CSA-H) shown in Figure 3b or of triangular shape (CSA-T) shown in Figure 3c.

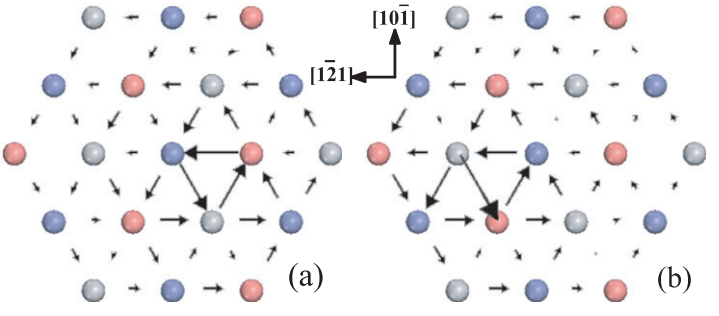

Figure 2. DD map of the core of the screw dislocation in Ta under (a) zero stress (left panel), and (b) 1.8 GPa (right panel). Circles of different color (grayscale) represent atoms on three successive (111) planes.

Table 1. Peierls stress (σ_P) and core structure for a screw dislocation in Ta using the present multiscale approach, the FP-GFBC method, the EAM, and the modified generalized pseudopotential theory (MGPT).

	σ_P (GPa)	Core structure
Present work	1.8	Non-degenerate
FP-GFBC [18]	1.8	Non-degenerate
EAM [19]	1.8	Degenerate
MGPT [20]	0.6	Non-degenerate

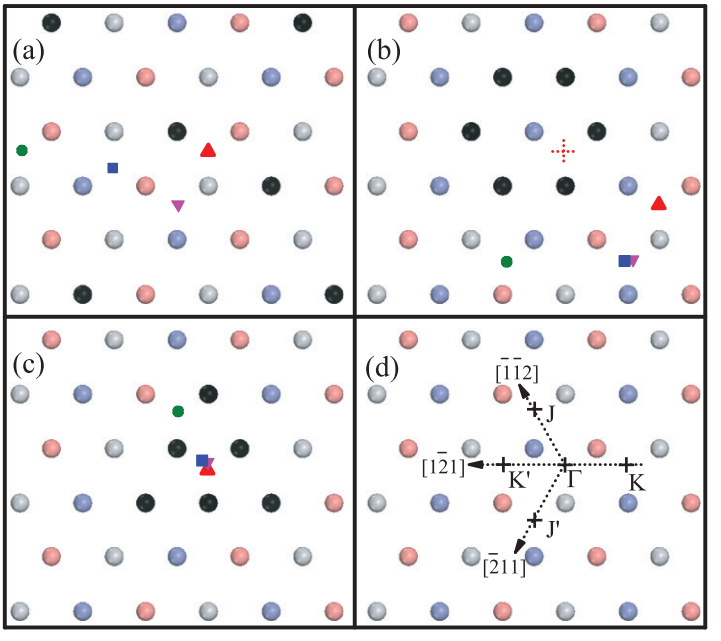

Figure 3. Screw dislocation slip paths under stress for three configurations of W solutes denoted by black circles: (a) isolated solute atoms (ISA); and nanoclusters of (b) hexagonal (CSA-H) or (c) triangular (CSA-T) shape. The upward triangle, downward triangle, square, and dot denote the position of the core center under 0.0, 1.0, 1.5, and 2.0 GPa, respectively. Panel (d) displays the special points and directions in Figure 4. Γ indicates the initial position of the dislocation.

In all cases the W concentration is ~6 at.%. ISA has the lowest energy in all the three configurations. CSA-H and CSA-T are higher by 0.34 eV and 0.48 eV, respectively. Thus none of these three configurations can be neglected to discuss the effects of W on the mobile properties of the screw dislocation. The W atoms are denoted with black circles. The upward triangle, downward triangle, square, and dot denote the position of the dislocation center under 0.0, 1.0, 1.5, and 2.0 GPa, respectively. In the absence of stress the core center is at point Γ in panel (d) for the ISA and the CSA-T cases, while it is unstable (dashed cross in panel (b)) for the CSA-H case. Interestingly, in the latter case the dislocation center is repelled by the CSA-H and spontaneously moves to the position of the upward triangle under the precipitate-induced chemical stress. Under 1.0 GPa, both in the ISA and CSA-H cases the dislocation prefers to bypass the W sites and moves on the $(0\bar{1}1)$ plane. Upon increasing the stress to 1.5 GPa, the behavior changes: the dislocation in ISA continues to move, while it is pinned in CSA-H. The dislocation in CSA-H begins to move further under 1.8 GPa, as in the case in pure Ta. In sharp contrast to the other two cases, the dislocation core is pinned at Γ in the CSA-T case until the stress reaches 2.0 GPa, where the center moves on the $(\bar{1}10)$ glide plane. The calculated values of critical stress, σ_P, and polarization [19], p, are listed in Table 2, for the ISA, CSA-H, and CSA-T environments. Both ISA and CSA-H result in SSS, while CSA-T

Table 2. σ_P (GPa) and polarization [19], p, for: isolated solute atoms (ISA), nanoclusters of solute atoms of hexagonal shape (CSA-H), or of triangular shape (CSA-T), shown in Figure 3.

	ISA	CSA-H	CSA-T
σ_P	1.0	1.0	2.0
p	0.10	0.04	0.00

produces SSH. In all cases, W solutes have a small effect on the polarization, indicating the absence of correlation between the polarization and σ_P.

Edagawa et al. suggested [21] that the dislocation motion in bcc metals can be represented by the Peierls potential surface (PPS), a 2D surface perpendicular to the Burgers vector. The profile of PPS is a valuable quantity to measure the lattice resistance to dislocation motion. Using the present approach we have determined the PPS by moving the dislocation center along four important directions in Figure 3d. The PPS along the various $\langle\bar{1}2\bar{1}\rangle$ directions for pure Ta, the ISA, and the CSA-T environments is shown in Figure 4a and the corresponding PPS for CSA-H is shown in Figure 4b. The Peierls barrier along the $[1\bar{2}1]$ (Γ-K′) and $[\bar{2}11]$ (Γ-J′) directions is reduced compared to pure Ta, consistent with the results of σ_P in Table 2. On the other hand, the CSA-H environment has a large effect on the PPS along the $[\bar{1}2\bar{1}]$ direction, where the Peierls barrier between Γ and K is greatly reduced, which means dislocation can glide to K very easily. The collapse of the Peierls barrier may contribute to the observation of spontaneous (under zero stress) gliding of the dislocation in Figure 3b. Finally, for the CSA-T configuration, the barrier along $[1\bar{2}1]$ on the $(\bar{1}01)$ plane increases, while that along $[\bar{1}\bar{1}2]$ on the $(\bar{1}10)$ plane remains the same as in Ta. Thus, the dislocation first glides on the $(\bar{1}10)$ plane, which is different from that in pure Ta.

In order to understand the underlying mechanism of the dislocation–solute interaction, we present in Figure 5 the change in energy, $\Delta E^{(\mathrm{X-X})}(\frac{u}{b})$, per unit length to displace an atomic row of X atoms (X = Ta, W) by u along $\langle 111\rangle$ relative to a nearest-neighbor Ta atomic row [3,4,22]. We find that W increases substantially the inter-row shear energies for the Ta-W and W-W rows and the lattice resistance when the dislocation center is in the vicinity of W. This in turn increases σ_P and hence SSH. On the other hand, the dislocation tends to bypass W and changes the slip plane and/or slip direction. This could be achieved by cross-slip. The definitive mechanism requires further study. The interplay between dislocation pinning, cross slip, and kink nucleation is responsible for the multitude of plastic behavior observed in solid-solution alloys.

4. Conclusion

In summary, we have employed a novel concurrent multiscale approach to study the effect of chemistry on the dislocation mobility in refractory bcc metals. The unique feature of this approach is that it correctly treats the long-range dislocation strain field, while allowing the quantitative treatment of the effect of chemistry on the

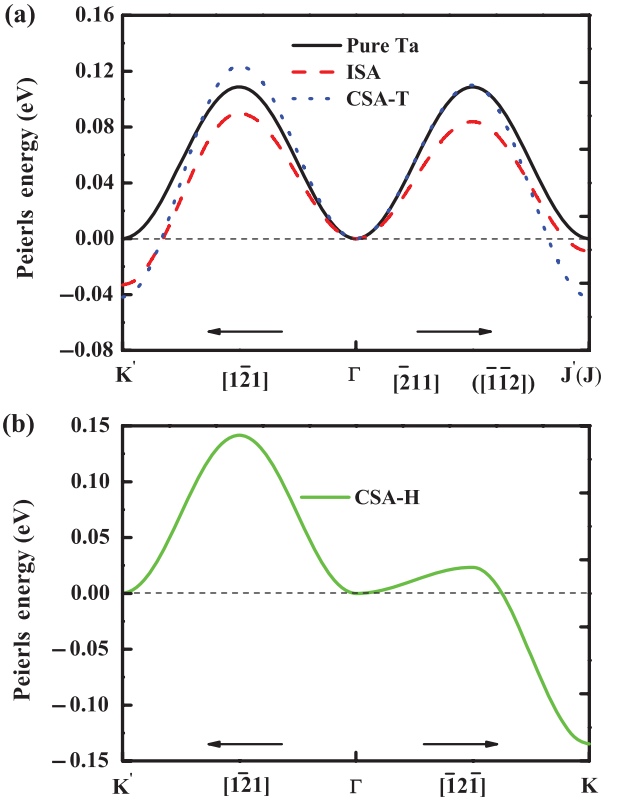

Figure 4. Peierls potential along the various $\langle 1\bar{2}1\rangle$ directions in Figure 3d for: (a) Pure Ta (solid curve), the ISA (dashed curve), and the CSA-T (dotted curve); and (b) for the CSA-H. The direction and special point in parenthesis in Figure 4a correspond to the CSA-T environment.

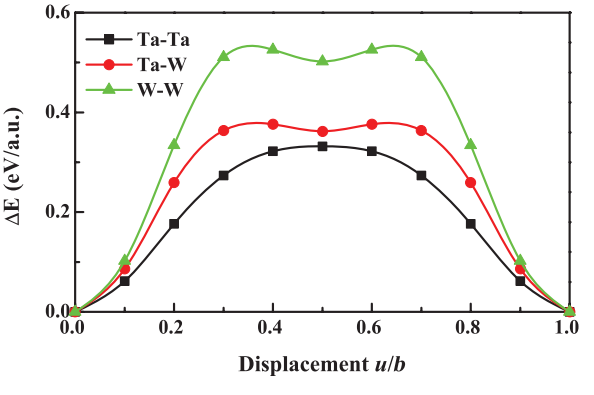

Figure 5. Energy change per unit length, $\Delta E^{(X-X)}(\frac{u}{b})$ (X = Ta, W), versus the normalized atomic-row displacement u/b along $\langle 111\rangle$.

dislocation core. The multiscale approach yields a core structure and dislocation mobility for Ta in excellent agreement with the FP-GFBC method [18]. We have demonstrated that the *local environment* of W solutes changes the anisotropy of the lattice resistance, and hence it has a large effect on both the dislocation mobility and slip paths: it may lead to SSS, SSH, or even a spontaneous dislocation glide.

Acknowledgements

We acknowledge valuable discussions with V. Vitek. This research was supported by a DOE NERI grant DE-FC07-06ID14748, NSF-PREM grant DMR-00116566, US Army grant W911NF-04-1-0058, and DOE SciDAC grant DE-FC02-06ER25791.

References

[1] E. Pink and R.J. Arsenault, Prog. Mater. Sci. 24 (1979) p.1.
[2] Y.F. Gu, H. Harada and Y. Ro, J. Metals 56 (2004) p.28.
[3] D.R. Trinkle and C. Woodward, Science 310 (2005) p.1665.
[4] N.I. Medvedeva, Yu.N. Gornostyrev and A.J. Freeman, Phys. Rev. Lett. 94 (2005) p.136402.
[5] W.H. Gourdin, D.H. Lassila, M.M. LeBlanc and A.L. Shields, J. de Physique IV, Colloque C8 (1994) p.207.
[6] C.L. Briant and D.H. Lassila, J. Eng. Mater. Tech. Trans. ASME 121 (1999) p.172.
[7] N. Choly, G. Lu, E. Weinan and E. Kaxiras, Phys. Rev. B 71 (2005) p.094101.
[8] Y. Liu, G. Lu, Z.Z. Chen and N. Kioussis, Model. Simul. Mater. Sci. Eng. 15 (2007) p.275.
[9] P.E. Blöchl, Phys. Rev. B 50 (1994) p.17953.
[10] G. Kresse and J. Furthmuller, Phys. Rev. B 54 (1996) p.11169.
[11] H.J. Monkhorst and J.D. Pack, Phys. Rev. B 13 (1976) p.5188.
[12] J.P. Perdew, K. Burke and M. Ernzerhof, Phys. Rev. Lett. 77 (1996) p.3865.
[13] S. Han, L. Zepeda-Ruiz, G. Ackland, R. Car and D. Srolovitz, J. App. Phys. 93 (2003) p.3328. See also http://homepages.ed.ac.uk/graeme.
[14] R.A. Johnson, Phys. Rev. B 39 (1989) p.12554.
[15] C. Domain and G. Monnet, Phys. Rev. Lett. 95 (2005) p.215506.
[16] J.P. Hirth and J. Lothe, *Theory of Dislocations*, 2nd ed., John Wiley, New York, 1982, p.68.
[17] V. Vitek, Cryst. Lattice Defects 5 (1974) p.1.
[18] C. Woodward and S.I. Rao, Phys. Rev. Lett. 88 (2002) p.216402.
[19] G. Wang, A. Strachan, T. Çağin and W.A. Goddard III, Mater. Sci. Eng. A 309 (2001) p.133.
[20] L.H. Yang, P. Söderlind and J.A. Moriarty, Phil. Mag. A 81 (2001) p.1355.
[21] K. Edagawa, T. Suzuki and S. Takeuchi, Phys. Rev. B 55 (1997) p.6180.
[22] Z.Z. Chen, N. Kioussis, N. Ghoniem and T. Hasebe, Phys. Rev. B 77 (2008) p.014103.